Breakup of the proton halo nucleus ^{8}B at a sub-Coulomb energy

K. Palli,[1,2] A. Pakou,[1,*] A. M. Moro,[3,4] P. D. O'Malley,[5] L. Acosta,[6,7] A. M. Sánchez-Benítez,[8] G. Souliotis,[2] E. F. Aguilera,[9] E. Andrade,[6] D. Godos,[6] O. Sgouros,[10,11] V. Soukeras,[10,11] C. Agodi,[10] T. L. Bailey,[5] D. W. Bardayan,[5] C. Boomershine,[5] M. Brodeur,[5] F. Cappuzzello,[10,11] S. Carmichael,[5] M. Cavallaro,[10] S. Dede,[5,12] J. A. Dueñas,[13] J. Henning,[5] K. Lee,[5] W. S. Porter,[5] F. Rivero,[5] and W. W. von Seeger[5]

[1]*Department of Physics and HINP, The University of Ioannina, 45110 Ioannina, Greece*

[2]*Department of Chemistry, National and Kapodistrian University of Athens and HINP, 15771 Athens, Greece*

[3]*Departamento de Física Atómica, Molecular y Nuclear, Universidad de Sevilla, Apartado 1065, E-41080 Sevilla, Spain*

[4]*Instituto Interuniversitario Carlos I de Física Teórica y Computacional (iC1), Apdo. 1065, E-41080 Sevilla, Spain*

[5]*Department of Physics and Astronomy, University of Notre Dame, Notre Dame, Indiana 46556, USA*

[6]*Instituto de Física, Universidad Nacional Autónoma de México, A.P. 20-364, Mexico City 01000, Mexico*

[7]*Instituto de Estructura de la Materia, CSIC, 28006 Madrid, Spain*

[8]*Departamento de Ciencias Integradas y Centro de Estudios Avanzados en Fisica, Matemáticas y Computación, Universidad de Huelva, 21071 Huelva, Spain*

[9]*Departamento de Aceleradores y Estudio de Materiales, Instituto Nacional de Investigaciones Nucleares, Apartado Postal 18-1027, Codigo Postal 11801, Mexico, Distrito Federal, Mexico*

[10]*INFN Laboratori Nazionali del Sud, via S. Sofia 62, 95125 Catania, Italy*

[11]*Dipartimento di Fisica e Astronomia"Ettore Majorana", Universita di Catania, via S. Sofia 64, 95125 Catania, Italy*

[12]*Cyclotron Institute, Texas A&M University, College Station, Texas 77843, USA*

[13]*Centro de Estudios Avanzados en Fisica, Matemáticas y Computación, Universidad de Huelva, 21071 Huelva, Spain*

(Received 6 December 2024; revised 7 January 2025; accepted 4 February 2025; published 18 February 2025)

We report inclusive breakup measurements of the proton halo nucleus ^{8}B on a medium mass target, ^{90}Zr. The experiment was carried out at the *TriSol* facility of the University of Notre Dame at a beam energy of 26.5 MeV, corresponding to 90% of the Coulomb barrier. The data include angular distributions of the ^{7}Be breakup fragment and of the elastically scattered ^{8}B nuclei, allowing a good normalization of the ^{7}Be yields. The latter are found to be in good agreement with the prediction of continuum-discretized coupled-channel calculations, thus pointing to the direct excitation to the continuum as the main production mechanism. The integrated breakup cross section, $\sigma_{bu} = 170 \pm 40$ mb, exhausts most of the total reaction cross section, indicating the dominance of direct processes below the barrier. A comparison of all existing breakup cross sections, on various targets at sub- and near-barrier energies, is also included.

DOI: 10.1103/PhysRevC.111.024615

I. INTRODUCTION

Studies with halo nuclei are challenging and offer the possibility to study exotic structures and unusual reaction mechanisms [1]. Halos are composed of one or more nucleons weakly bound to a nucleus core. The dilute density distribution, which is formed in that way, extends their size much further than the radius expected for a well-bound nucleus. The halo nucleons are well embedded in a classically forbidden region and live there due to the quantum tunneling effect. The excitation scheme of such nuclei is formed by a continuum of states, which provides a large environment for interactions and a good example of an open quantum system [2]. Coupling to this environment may alter standard results in processes such as elastic scattering and reactions like fusion. Therefore, breakup plays an important role in understanding structure properties of these nuclei, such as ground-state and continuum spectroscopic properties and the dynamics of nuclear reactions.

Neutron halo nuclei, such as ^{6,8}He, ^{11}Be, ^{11}Li, are mostly studied, exhibiting remarkable coupling effects at near- and sub-barrier energies [3–7]. All of them have small binding energies and the valence neutrons have low or no orbital angular momentum, avoiding any inhibition of the tunneling effect due to the centrifugal barrier. For proton halo nuclei, the manifestation of the halo can be observed in reaction dynamics despite the proton-core or proton-target Coulomb interaction at the expense of low binding energies. Calculations within this motivation underline the equivalence between a neutron halo nucleus of higher binding energy and a proton halo nucleus with lower breakup energy [8,9]. Then, similar effects are expected in collisions involving *n*-halo or *p*-halo nuclei. In fact, in a phenomenological approach to determine the reduced interaction distance of ^{8}B and other weakly bound nuclei on various targets, through elastic scattering measurements and optical model analysis, this similarity was observed between ^{8}B and ^{6}He nuclei. They exhibit the same reduced

*Contact author: apakou@uoi.gr

interaction radius as well as the same reduced total reaction cross section [10].

^{8}B is a very challenging nucleus with five protons and only three neutrons, with a proton halo outside of a ^{7}Be core, and a very small binding energy of 0.136 MeV. This nucleus is a very appealing case both for exploring its continuum excitations and the consequences on coupling mechanisms to continuum, as well as for its role in the high-energy neutrino flux produced in the sun. Accurate measurements of the capture reaction ^{7}Be$(p,\gamma)^{8}$B cross section are of major importance, to validate theoretical predictions of solar models [11–13] and to constrain terrestrial measurements on the solar neutrino flux [14–17]. A history of direct and indirect measurements of the above reaction and their drawbacks are described in detail in Ref. [13]. In the list of indirect measurements more relevant to this work is the breakup of ^{8}B on a ^{58}Ni target [18,19] at sub-Coulomb energies, but which failed to discriminate between $E1$ and $E2$ multipolarities and therefore did not determine the astrophysical S factor, S_{17}, for proton capture on ^{7}Be at solar energies. In principle, the ^{8}B breakup at sub-Coulomb energies should be a good indirect method to study the above reaction. However, the low flux of the ^{8}B beams, which does not allow exclusive measurements, and the poor collimation of the secondary beams, which does not allow measurements at angles close to zero degrees, both issues prerequisites for extracting the rate of the proton capture reaction [20], do not provide the necessary experimental conditions.

Motivated by the above, we previously performed a breakup measurement of ^{8}B on the heavy target, ^{208}Pb, at deep sub-barrier energies [21]. The breakup cross section was found to be very large, $\sigma_{\rm bu} = 326 \pm 84$ mb and equal within error bars with the total reaction cross section, exhausting all other reaction channels. At much higher energies, around 4 times the Coulomb barrier, a large breakup cross section of $\sigma_{\rm bu} = 779$ mb was also reported [22], to be compared with a total reaction cross section of 3423 mb. Both of them were in accordance with a phenomenological prediction for the ratio of direct channel cross sections versus the total reaction cross section as a function of energy, based on measurements of fusion and total reaction cross section below and above the barrier energies [23]. According to this, at the above barrier energies, the ratio is almost constant and close to 20%, while approaching the barrier, an increase is observed but with different slopes for light, medium and heavy targets. Below barrier the ratio saturates to 100% for heavy targets, while for medium mass a value of 80% and finally for a light target a value of 75% is reached. The below-barrier region is mostly unexplored and the prediction is based on extrapolations from weakly bound but stable nuclei. For that, it presents strong interest [24]. Therefore, in continuation of the breakup measurement on lead [21], we present in this paper similar measurements, but for the medium-mass target ^{90}Zr. The beam energy now is not at deep sub - barrier energies, but it is well below the barrier at 26.5 MeV corresponding to $\approx 90\%$ of it ($E_{\rm C.b.} = 30.4$ MeV).

Very recently a new measurement has appeared in the literature, in relation with the inclusive breakup of ^{8}B on a ^{208}Pb target at a barrier energy and will also be discussed in this paper [25].

In the following, in Sec. II, we present the experimental details and our data results In Sec. III is our theory with continuum-discretized coupled-channel (CDCC) calculations. Finally in Sec. IV is the discussion with our conclusions.

II. EXPERIMENTAL DETAILS AND RESULTS

The experiment was performed at the newly upgraded radioactive beam facility *TriSol* [26] of the University of Notre Dame. Details of the experiment are given in Refs. [10,27], where the elastic scattering of ^{7}Be + $^{\rm nat}$Zr and ^{8}Be + $^{\rm nat}$Zr are presented, with data collected under the same experimental conditions.

The secondary ^{8}B beam was produced in-flight, as part of a cocktail beam together with ^{7}Be and ^{7}Li. The reaction used was ^{3}He + ^{6}Li with the two proton transfer channel ^{3}He(^{6}Li, n)^{8}B, leading to ^{8}B. A primary bunched beam of ^{6}Li was accelerated at 37 MeV by the UND FN tandem, and impinged on a 2.5 cm long gas target of ^{3}He at a pressure of 850 Torr. Secondary beams were focused and guided by the three superconducting solenoids to a $^{\rm nat}$Zr target of 1.95 mg/cm^2 thickness. In the middle of the target, the beam energies corresponded to 26.5 MeV, 19.2 MeV, and 14.3 MeV for ^{8}B, ^{7}Be, and ^{7}Li, respectively. The reaction products, including elastically scattered particles, were detected in four two-stage ΔE-E telescopes with a DSSSD detector (double-sided silicon strip detector) as ΔE, 15 to 20 μm thick and as E a silicon pad 130 to 500 μm thick. Two of the telescopes were installed at forward angles ($\theta_{\rm lab} \sim 20^\circ$ to 60°) at symmetrical positions, correcting for beam divergence. The other two were installed backwards again at symmetrical positions, covering an angular range of $\theta_{\rm lab} \sim 110^\circ$ to 150°. The telescopes were positioned at ~ 60 mm from the target. In this respect, each strip spanned an angular range of 3°, and therefore for each angle an uncertainty of 1.5° can be considered in the definition of angles in this work. The elastically scattered ^{8}B nuclei, used here for normalization purposes, were very well separated from the other beam products with the ΔE-E technique, as can be seen in Fig. 1. We should also note that for the needs of this experiment only the forward telescopes were used, since at backward angles the statistics of breakup drops rapidly.

For the breakup measurement, an unambiguous separation has to be obtained between the ^{7}Be fragments resulting from ^{8}B breakup and the ^{7}Be contamination in the secondary beam, elastically scattered by the $^{\rm nat}$Zr target. This was achieved for a very small part of the data with a time-of-flight (TOF) technique which was imposed between the start of the DSSSD detectors and the radio frequency of the pulsed beam. Preliminary results are presented in Ref. [28], but with very large uncertainties. However, for the majority of the data that are presented here, the time separation was not unambiguous, and we had to consider the kinematics of the reactions. Fortunately, the experimental energy distribution of the elastically scattered ^{7}Be beam on the $^{\rm nat}$Zr target, was partially overlapped with the energy distribution of breakup events, as can be seen in Fig. 2. In this figure, the calculated energy distribution of the ^{7}Be breakup fragments, is compared with the energy distribution of the elastically scattered particles due to the beam contamination, taking into account the energy loss

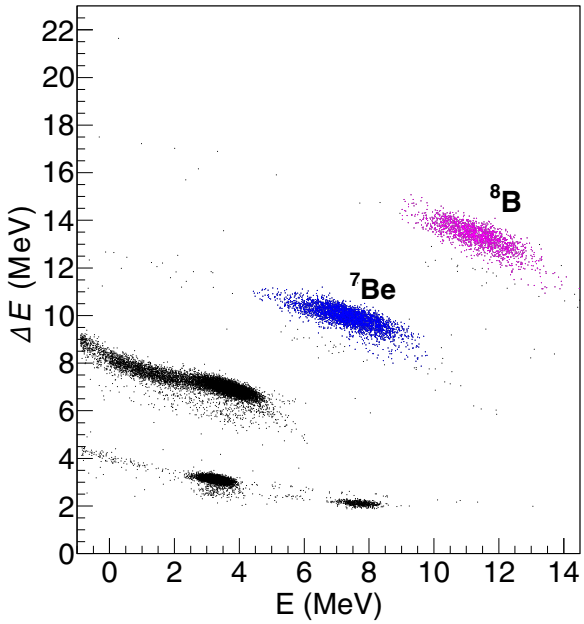

FIG. 1. Spectrum of ΔE versus E from one of the forward-angle telescopes. Data were collected by a middle strip corresponding to an angle $\theta_{\rm lab} = 25 \pm 1.5^{\circ}$. The figure is from Ref. [10].

due to the finite thickness of the target. The overlap between the breakup fragments and the beam contamination particles is larger for the more backward angles than the more forward ones.

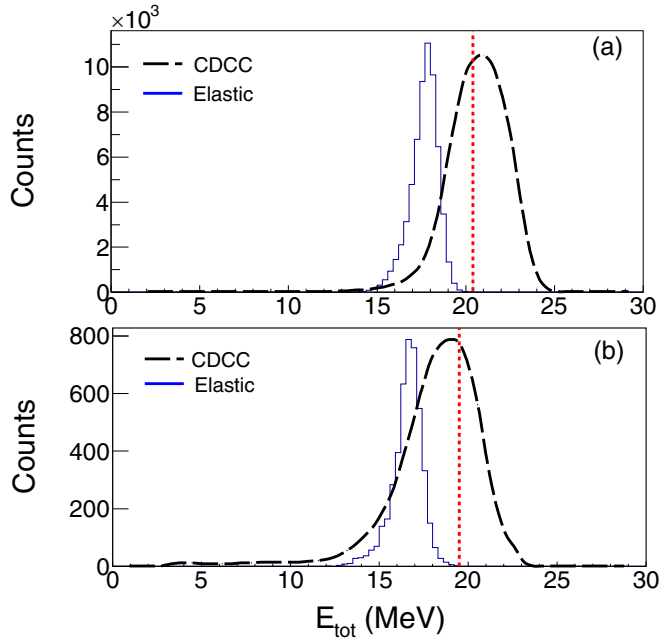

FIG. 2. Breakup energy distributions for ^{7}Be fragments following the ^{8}B projectile breakup, calculated with the CDCC formalism, are compared with the experimentally determined elastic scattering distribution of the contaminant ^{7}Be beam at two angles (a) 28.4° and (b) 54.7°. The vertical line indicates the threshold energy above which breakup data are considered.

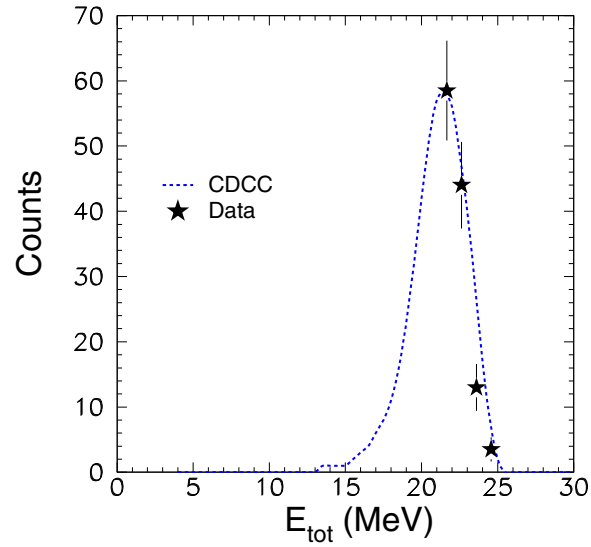

FIG. 3. The energy distribution of the ^{7}Be breakup fragments, observed in the angular range of the present experiment, 20° to 58°. Our experimental data are designated with the stars, and are compared with our CDCC calculations, designated with the dotted blue line.

To unambiguously extract the breakup yields, a threshold above the overlap was imposed as demonstrated in Fig. 2 with the vertical dotted red line. Such energy distributions with the appropriate thresholds were used for the determination of the breakup yields. Recovery of missing counts was achieved by integrating the energy spectra and forming the ratio of the breakup area above the energy threshold versus the total energy distribution area (recovery ratio). Energy distributions were adopted by means of CDCC calculations, to be described below. The use of calculated energy distributions was validated by comparing experimental data and calculations, as it is demonstrated in Fig. 3, where very good agreement is observed. The so-obtained breakup yields were normalized taking into account the elastic scattering events at those angles, where the scattering follows the Rutherford behavior. In this regard, differential breakup cross sections $\mathrm{d}\sigma(\theta)/\mathrm{d}\Omega$ and breakup probabilities, $P(\theta)$, were calculated as follows:

$$\left(\frac{d\sigma(\theta)}{d\Omega}\right)_{\rm break} = P_{\rm break}(\theta)\frac{d\sigma_{\rm el}(\theta)}{d\Omega} \tag{1}$$

with

$$P_{\rm break}(\theta) = \frac{N_{\rm break}(\theta)}{N_{\rm el}(\theta)}, \tag{2}$$

where $N_{\rm break}(\theta)$, $N_{\rm el}(\theta)$, and $d\sigma(\theta)_{\rm el}/d\Omega$ are the breakup yields, the elastic scattering yields and the Rutherford cross section at an angle θ, respectively. The results are presented in Fig. 4. It should be underlined here that by using elastic scattering for normalization, all uncertainties due to target thickness, solid angle, and flux are eliminated. The systematic uncertainties in this experiment were mainly due to statistics (∼18%) and due to the recovery ratio applied in the measured breakup yield (∼20%), for the last taking into account a 1%

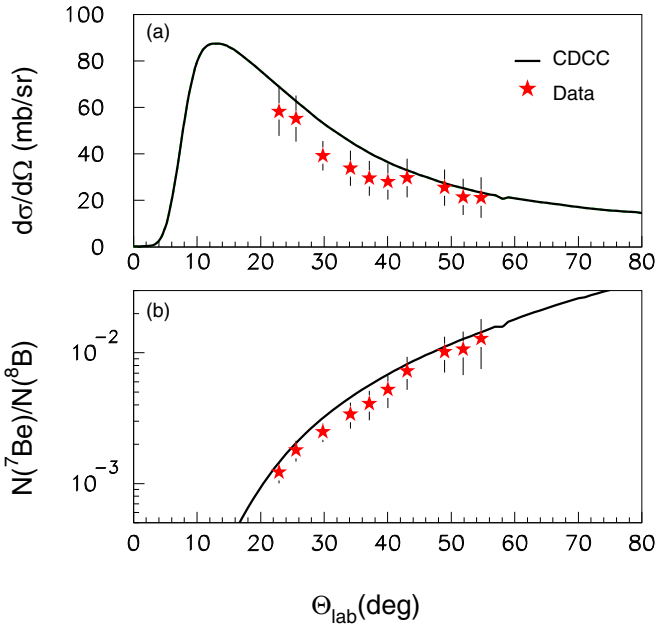

FIG. 4. (a) Breakup differential angular distribution for $^{8}\mathrm{B}+^{90}\mathrm{Zr}$ at 26.5 MeV and (b) Breakup probability for the same system. The experimental data are compared with theoretical CDCC calculations, shown with the black solid line. Error bars assigned to the data are only due to statistics—see text for further explanations.

error in the definition of the threshold energy. As explained above, the recovery ratio is formed as the ratio of the breakup area above the energy threshold versus the total energy distribution area—see Fig. 2. Uncertainties due to secondary beam divergence were eliminated, by taking the mean between differential cross sections of left and right detectors to the incident beam, installed at symmetrical positions.

III. THEORETICAL ANALYSIS

The measured ^{7}Be angular and energy distributions have been compared with theoretical calculations. Since the measurements are inclusive with respect to the protons emitted following the projectile breakup, two distinct contributions are possible. On the one hand, we have the involvement of elastic breakup events (EBU). These correspond to the projectile dissociation without capture of the proton by the target and which remain in the ground state. On the other hand, we have nonelastic breakup events (NEB), accompanied by target excitation or proton capture by the target. The two contributions, EBU and NEB, have been separately evaluated, by using the CDCC and the Ichimura-Austern-Vincent (IAV) methods [29,30], respectively, as described in the following subsections.

A. CDCC calculations

CDCC calculations have been performed assuming a three-body model for the reaction ($^{7}\mathrm{Be}+p+^{90}\mathrm{Zr}$). These calculations follow closely those presented in Ref. [27] for the elastic channel, but are summarized here for completeness. The $^{7}\mathrm{Be}+p$ interaction, required to generate the ground and continuum states of ^{8}B, was taken from [31]. It contains both central and spin-orbit terms. The ^{7}Be spin was ignored for simplicity. The ground state was assumed to consist of a pure $1p_{3/2}$ configuration. The $p+^{90}$Zr potential was taken from the global parametrization of Koning-Delaroche [32]. The $^{7}\mathrm{Be}+^{90}\mathrm{Zr}$ potential was computed from a double-folding calculation using a BDM3Y1 nucleon-nucleon interaction and scaled by the factors $N_r = 1.2$ $N_i = 0.476$ deduced from elastic scattering data of $^{7}\mathrm{Be}+^{90}\mathrm{Zr}$ measured in the same experiment. Details can be found in [10]. The ^{8}B unbound states were represented by a set of $^{7}\mathrm{Be}+p$ continuum bins up to a maximum energy $\varepsilon_{\max} = 9$ MeV and a maximum orbital angular momentum $\ell_{\max} = 6$. The coupling potentials included both nuclear and Coulomb couplings. The calculations were performed with the code FRESCO [29].

For comparison with the experimental data, double differential cross sections as a function of the energy and angle of the ^{7}Be were obtained by a suitable kinematical transformation of the breakup scattering amplitudes, following the formalism and codes of Ref. [33]. The calculated ^{7}Be energy distributions are compared with the measured elastic peak in Fig. 2 and with the measured ^{7}Be distributions in Fig. 3 and the energy-integrated ^{7}Be angular distributions are compared with the data in Fig. 4. Note that, since the protons are not observed, these elastic breakup observables are integrated over all proton angles.

B. Nonelastic breakup contributions

The nonelastic breakup contribution (NEB) to the inclusive breakup cross section, has been estimated with the IAV model [30]. This model has been successfully applied before to other inclusive breakup reactions, induced by weakly bound projectiles, including deuterons, ^{6,7,8}Li and ^{8}B [22,34]. The calculation is based on the DWBA approximation and therefore requires optical potentials for the entrance ($^{8}\mathrm{B}+^{90}\mathrm{Zr}$) and exit ($^{7}\mathrm{Be}+^{91}\mathrm{Nb}*$) channels. The other required potentials, such as the $p+^{7}$Be and p+ ^{90}Zr potentials, are the same as those employed in the CDCC calculations. These calculations were performed with the SMOOTHIE code [35]. The obtained angular distribution is shown in Fig. 5 in the entire angular range. It can be seen that the NEB contribution is more substantial at backward angles. However, the total integrated NEB cross section is 22 mb, and only comprises ∼10% of the total breakup.

Therefore, we conclude that for the present system at below barrier energies, elastic breakup is the dominant mechanism contributing to the inclusive breakup. This is in accordance with previous calculations for $^{8}\mathrm{B}+^{58}$Ni [33].

IV. DISCUSSION AND CONCLUSIONS

We have measured the breakup of the proton halo nucleus ^{8}B on a medium mass target, ^{90}Zr. It should be noted that a natural target was employed; however, we may anticipate that this does not impact the conclusions, as we do not expect a significant dependence of the breakup on the specific isotope. The study was performed at the rather low energy of 26.5 MeV, which corresponds to ∼90% of the Coulomb

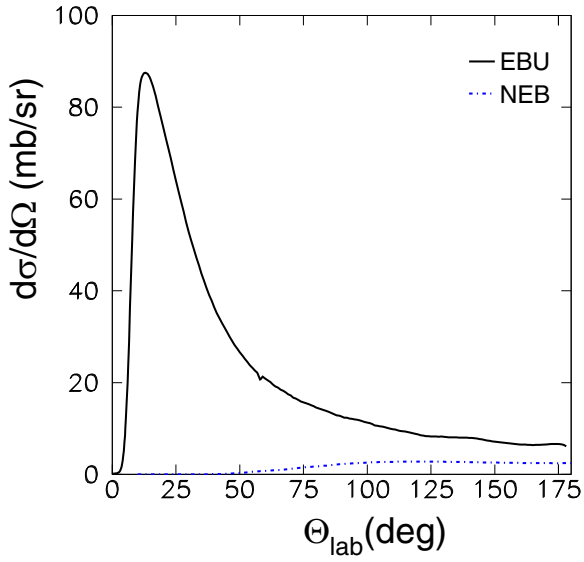

FIG. 5. Calculated differential angular distributions for the inclusive ^{7}Be production in the reaction $^{8}\mathrm{B}+{}^{90}\mathrm{Zr}$ are presented for the whole angular range. The elastic breakup (EBU) according to CDCC calculations is denoted with the solid black line, while the nonelastic breakup (NEB) according to IAV calculations with the dotted-dashed blue line. It is obvious that NEB is substantial only at very large angles, outside the range covered by the present experiment.

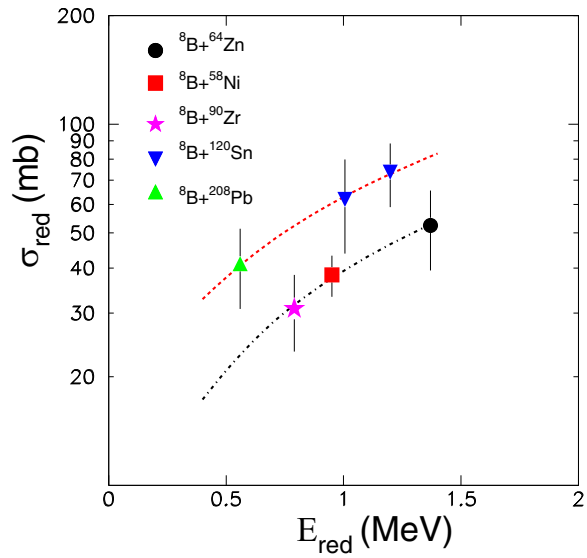

FIG. 6. Excitation functions of reduced breakup cross sections according to the prescription of Ref. [36] for the systems, indicated in the legend (see text for the reduction form). Breakup cross sections are taken from Refs. [2,18,21,34] and present measurement (star). Error bars for breakup cross sections for targets Zn, and Sn were not given by the authors of Refs. [2,34] and were estimated in this work, by taking into account the angular distributions reported therein. All error bars are due to statistics. The lines are best fits to the data, to guide the eye.

barrier. Differential cross section angular distributions and probabilities of the ^{7}Be fragments were deduced and compared with CDCC calculations based on a three-body model of the reaction. Experimental data and calculations were found to be in good agreement.

Nonelastic breakup contributions, which might be present in the data due to its inclusive character, were estimated with the IAV model [30] and found to be negligible within the measured angular range.

This measurement follows a series of low-energy breakup experiments, performed at the Notre Dame radioactive facility. The first one, was performed with a ^{58}Ni target, at a close barrier energy of 25.8 MeV ($E^{\mathrm{lab}}_{\mathrm{C.b.}} = 23.7\,\mathrm{MeV}$), followed by one at a deep sub-barrier energy on a ^{208}Pb target at 30 MeV ($E^{\mathrm{lab}}_{\mathrm{C.b.}} = 51.6\,\mathrm{MeV}$), and the present one on a ^{90}Zr target at the sub-Coulomb energy of 26.5 MeV ($E^{\mathrm{lab}}_{\mathrm{C.b.}} = 30.4\,\mathrm{MeV}$).

For drawing conclusions through systematics, the breakup cross sections for all the above systems and for ^{120}Sn and ^{64}Zn targets performed in other laboratories [22,34], are plotted in a reduced form in Fig. 6, according to the prescriptions described in Ref. [36]. That is, replacing breakup cross sections and center of mass energies with the quantities: $\sigma^{\mathrm{red}}_{\mathrm{break}} = \sigma_{\mathrm{break}}/(A_p^{1/3} + A_t^{1/3})$ and $E_{\mathrm{red}} = E_{\mathrm{c.m.}}(A_p^{1/3} + A_t^{1/3})/(Z_p Z_t)$. In addition, in Fig. 7, cross sections are plotted as a function of the head-on distance of the closest approach D_0. A very interesting behavior is observed from both plots. Breakup cross sections for lighter targets up to ^{90}Zr appear to lie on the same smooth curve, while those for heavier targets (from ^{120}Sn to ^{208}Pb) follow a different curve. The same trend is observed if the reduction is applied according to Ref. [37]. The assigned errors due to statistics are large and they can

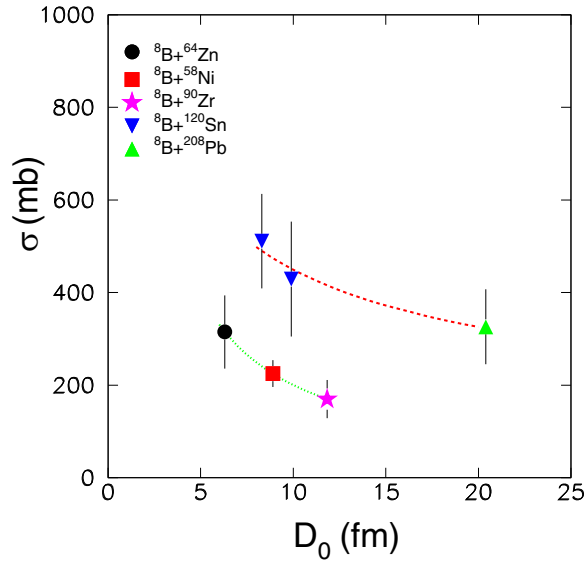

FIG. 7. Excitation functions of breakup cross sections versus the head-on collision distances, for the systems indicated in the legend. Breakup cross sections are taken from Refs. [2,18,21,34] and the present work (star). Error bars for breakup cross sections for targets Zn, and Sn were not given by the authors of Refs. [2,34] and were estimated in this work, by taking into account the angular distributions reported therein. All error bars are due to statistics. The lines are best fits to the data, to guide the eye.

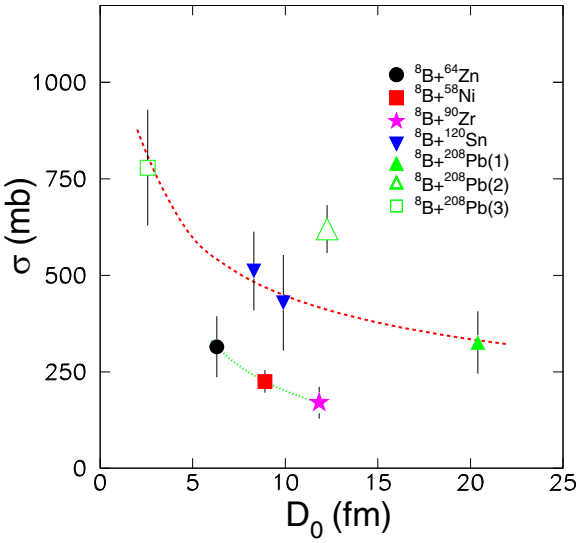

FIG. 8. Same as in Fig. 7, but including data with energies at barrier (Ref. [25]) and 4 times the barrier (Ref. [22]), designated with the open triangle and the open box, respectively. Indexes (1), (2), and (3) for the lead target refer to our previous measurement [21], the very recent measurement at barrier [25] and the higher energy measurement [22], respectively. Error bars for breakup cross sections for targets Zn, Sn, Pb(2) (at the barrier energy) and Pb(3)(at the highest energy) were not given by the authors of Refs. [2,22,25,34] and were estimated in this work, by taking into account the angular distributions reported therein. The lines are best fits to the data, to guide the eye.

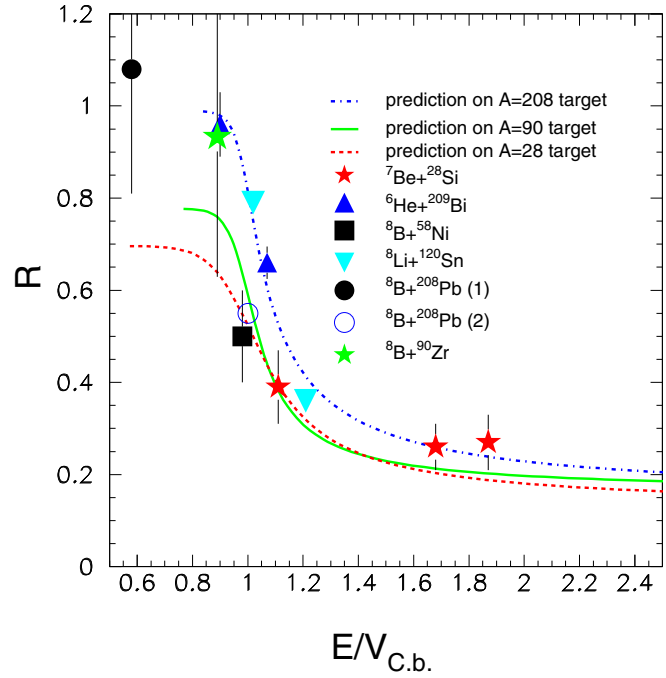

FIG. 9. Ratios of cross sections: direct to total, for various weakly bound projectiles on various targets. The lines are predictions from systematics [23]. More details about the systems are given as an inset. Data are from Refs. [18,40–42] for Si, Ni, Sn, Bi targets, respectively, and for Pb(1) from Ref. [21], and Pb(2) from Ref. [25].

be larger if we add up systematic uncertainties. Therefore the existing information neither in experiment nor in theory is adequate to make firm conclusions about this observation. If this differentiation is due to different coupling mechanisms, then it could be relevant to a differentiation between light and heavy targets which was already reported in Ref. [38]. This had to do with the energy dependence of the optical potential at sub- and near- barrier energies with consequences on coupling mechanisms and the sub- barrier fusion. Additionally in Ref. [39] a differentiation between incomplete fusion for light versus heavy targets is also reported.

We will consider now the very recent measurement of $^{8}\mathrm{B} + ^{208}\mathrm{Pb}$ at the barrier energy of 50 MeV, performed at the CNS Radioactive Ion Beam facility of the University of Tokyo [25]. The result, together with the datum for the same system but at a much higher energy of 238 MeV (4 times the Coulomb barrier), performed at the Heavy-Ion Research Facility in Lanzhou [22], is presented in Fig. 8. It is interesting to note that the measurement at the barrier energy [25] is much higher than all other measurements. Although the breakup from this measurement was found to be in agreement with the prediction of a CDCC calculation [25], further work is needed to elucidate why the ^{7}Be yield from this reaction is significantly higher than that from our ^{8}B reaction on Pb and other targets. We should note here that only for the lead target we have measurements and calculations in a broad energy range. Within the very recent work and according to the calculations, a large direct breakup channel is observed which remains almost constant from the Coulomb barrier energy up to 4 times the Coulomb barrier. If this is a phenomenon seen only for the lead target or not has to be investigated in the future with more breakup measurements and calculations at sub- and especially at near-barrier energies, with a lead target or/and with various targets.

The total experimental breakup cross section for the present system $^{8}\mathrm{B} + ^{90}\mathrm{Zr}$, was found to be $\sigma_{\mathrm{break}} = 170 \pm 40$ mb. This result was obtained by integrating the experimental angular distribution, but assuming the same shape as in the CDCC calculation for all missing angles. This value is close to the total reaction cross section, extracted from an OMP (Optical Model Potential) analysis of elastic scattering data [10], $\sigma_{\mathrm{reac}} = 180 \pm 40$ mb. The ratio of direct cross sections versus the total reaction cross section, is found to be $R = 0.95 \pm 0.23$ roughly following the trend found for a ^{208}Pb target at deep sub-barrier energies (see Fig. 9). However, because of the large assigned error, we cannot exclude agreement with the systematics for weakly bound but stable projectiles on medium-mass targets. In the last case, the deduced value, extracted mainly from extrapolations, was found to be $R = 0.8$. In any case, based on the existing data, a solid statement can be made that in reactions for halo nuclei and for energies below the barrier, the reaction cross section is dominated by the direct reaction component.

In summary, from the combined analysis of the present data along with existing data for the same projectile, we may extract the following conclusions

(i) New inclusive breakup measurements were obtained at a sub-barrier energy for a proton halo nucleus, ^{8}B,

at a medium mass target, ^{90}Zr. The results were found to be in good agreement with the CDCC calculations. These calculations confirm that the main mechanism in inclusive breakup is the elastic one, with NEB being negligible.

(ii) The comparison of the present breakup measurement with the total reaction cross section confirms once more the dominance of direct processes at below barrier energies for the proton halo nucleus ^{8}B, in accordance with phenomenological systematics.

(iii) Comparisons of ^{8}B breakup cross sections on various targets at sub- and near- barrier energies as a function of either energy in a reduced form or distance of closest approach, were attempted. It was observed a variation between light and heavy targets. The origin of this difference is unclear with the information collected so far, and needs further clarification.

ACKNOWLEDGMENTS

We warmly acknowledge technical support from the personnel of the radioactive beam facility of the University of Notre Dame and M. Pérez-Vielma from the Autonomous University of Mexico, for her technical support in the construction of the geometry used for the SIMAS+LIFE array, the detection telescopes used for the present measurements. We acknowledge support from NSF Grants No. PHY-2011890 and No. PHY-2310059 of the University of Notre Dame. One of us (K.P.) acknowledges support by the Hellenic Foundation for Research and Innovation (HFRI) under the 4th Call for HFRI PhD Fellowships, No. 009194, one (A.M.M.) is supported by MCIN/AEI/10.13039/501100011033, Grant No. PID2020-114687GB-I00, and one (L.A.) by CONAHCyT ApoyosLNC-2023-58 and DGAPA-PAPIIT IG101423.

[1] T. Nakamura and Y. Kondo, *Clusters in Nuclei*, Lecture Notes in Physics, edited by C. Beck (Springer, Berlin, Heidelberg, 2012), Vol. 848, p. 67.

[2] L. Yang, C. J. Lin, H. Yamahuchi, A. M. Moro, N. R. Ma *et al.*, Breakup of the proton halo nucleus ^{8}B near barrier energies, Nat. Commun. **13**, 7193 (2022).

[3] O. R. Kakuee, M. A. G. Alvarez, M. V. Andrés, S. Cherubini, T. Davinson *et al.*, Long range absorption in the scattering of ^{6}He on ^{208}Pb and ^{197}Au at 27 MeV, Nucl. Phys. A **765**, 294 (2006).

[4] L. Acosta, A. M. Sánchez-Benítez, M. E. Gómez, I. Martel, F. Pérez-Bernal *et al.*, Elastic scattering and α-particle production in ^{6}He + ^{208}Pb collisions at 22 MeV, Phys. Rev. C **84**, 044604 (2011).

[5] A. Di Pietro, G. Randisi, V. Scuderi, L. Acosta, F. Amorini *et al.*, Elastic scattering and reaction mechanisms of the halo nucleus ^{11}Be around the Coulomb barrier, Phys. Rev. Lett. **105**, 022701 (2010).

[6] N. Keeley, N. Alamanos, K. W. Kemper, and K. Rusek, Strong nuclear couplings as a source of Coulomb rainbow suppression, Phys. Rev. C **82**, 034606 (2010).

[7] M. Cubero, J. P. Fernández-García, M. Rodríguez-Gallardo, L. Acosta *et al.*, Do halo nuclei follow Rutherford elastic scattering at energies below the barrier? The Case of ^{11}Li, Phys. Rev. Lett. **109**, 262701 (2012).

[8] A. Bonaccorso, D. M. Brink, and C. A. Bertulani, Proton vs neutron halo breakup, Phys. Rev. C **69**, 024615 (2004).

[9] R. Kumar and A. Bonaccorso, Dynamical effects in proton breakup from exotic nuclei, Phys. Rev. C **84**, 014613 (2011).

[10] K. Palli, A. Pakou, P. D. O'Malley, L. Acosta, A. M. Sánchez-Benítez, G. Souliotis, A. M. Moro, E. F. Aguilera, E. Andrade, D. Godos, O. Sgouros, V. Soukeras, C. Agodi, T. L. Bailey, D. W. Bardayan, C. Boomershine, M. Brodeur, F. Cappuzzello, S. Carmichael, M. Cavallaro, S. Dede, J. A. Duenas, J. Henning, K. Lee, W. S. Porter, F. Rivero, and W. von Seeger, Elastic scattering of ^{8}B + ^{nat}Zr at the sub- barrier energy of 26.5 MeV, Phys. Rev. C **109**, 064614 (2024).

[11] J. N. Bahcall and M. H. Pinsonneanlt, Standard solar models, with and without helium diffusion, and the solar neutrino problem, Rev. Mod. Phys. **64**, 885 (1992).

[12] J. N. Bahcall, A. M. Serenelli, and S. Basu, Standard solar models: A Monte Carlo simulation, Astrophys. J. Suppl. Ser. **165**, 400 (2006).

[13] E. G. Adelberger *et al.*, Solar fusion cross sections. II. The pp chain and CNO cycles, Rev. Mod. Phys. **83**, 195 (2011).

[14] K. S. Hirata *et al.*(KamiokaNDE Collaboration), Observation of 8B solar neutrinos in the Kamiokande-II detector, Phys. Rev. Lett. **63**, 16 (1989).

[15] J. P. Cravens *et al.*(SuperKamiokaNDE Collaboration), Solar neutrino measurements in Super-Kamiokande-II, Phys. Rev. D **78**, 032002 (2008).

[16] B. Aharmim *et al.*(SNO Collaboration), Determination of the ν_e and total ^{8}B solar neutrino fluxes using the Sudbury Neutrino Observatory, Phase I data set, Phys. Rev. C **75**, 045502 (2007).

[17] M. Anderson *et al.*, Measurement of the ^{8}B solar neutrino flux in SNO+ with very low backgrounds, Phys. Rev. D **99**, 012012 (2019).

[18] V. Guimarães, J. J. Kolata, D. Peterson, P. Santi, R. H. White-Stevens, S. M. Vincent, F. D. Becchetti, M. Y. Lee, T. W. O'Donnell, D. A. Roberts, and J. A. Zimmerman, Nuclear and Coulomb interaction in ^{8}B breakup at sub-Coulomb energies, Phys. Rev. Lett. **84**, 1862 (2000).

[19] J. J. Kolata, V. Guimarães, D. Peterson, P. Santi, R. H. White-Stevens *et al.*, Breakup of ^{8}B at sub-Coulomb energies, Phys. Rev. C **63**, 024616 (2001).

[20] A. Tumino, C. Spitaleri, C. Bertulani, and A. M. Mukhamedzhanov, Nuclear astrophysics from view point of few-body problems, Few-Body Syst. **54**, 869 (2013).

[21] A. Pakou, L. Acosta, P. D. O'Malley, S. Aguilar, E. F. Aguilera *et al.*, Dominance of direct reaction channels at deep sub-barrier energies for weakly bound nuclei on heavy targets: The case ^{8}B + ^{208}Pb, Phys. Rev. C **102**, 031601(R) (2020).

[22] K. Wang, Y. Y. Yang, A. M. Moro, V. Guimarães, J. Lei, D. Y. Pang, F. F. Duan, J. L. Lou, J. C. Zamora, J. S. Wang, Z. Y. Sun, H. J. Ong, X. Liu, S. W. Xu, J. B. Ma, P. Ma, Z. Bai, Q. Hu, X. X. Xu, Z. H. Gao, G. Yang, S. Y. Jin, Y. H. Zhang, X. H. Zhou, Z. G. Hu, and H. S. Xu, Elastic scattering and breakup reactions of the proton drip-line nucleus ^{8}B on ^{208}Pb at 238 MeV, Phys. Rev. C **103**, 024606 (2021).

[23] A. Pakou, D. Pierroutsakou, M. Mazzocco, L. Acosta, X. Aslanoglou *et al.*, Total reaction cross sections for ^{8}Li + ^{90}Zr at near-barrier energies, Eur. Phys. J. A **51**, 55 (2015).

[24] A. Pakou, P. D. O'Malley, L. Acosta, A. M. Sánchez-Benítez, J. J. Kolata, K. Palli, O. Sgouros, V. Soukeras, and G. Souliotis, Searching for treasures at sub-barrier energies: The case of ^{8}B and ^{7}Be, Eur. Phys. J.-Web Conf. **252**, 04006 (2021).

[25] M. Mazzocco, N. Keeley, A. Lagni, A. Boiano, C. Boiano *et al.*, Inclusive ^{7}Be production cross section in the ^{8}B + ^{208}Pb system at the Coulomb barrier, Phys. Rev. C **110**, 044611 (2024).

[26] P. D. O'Malley, T. Ahn, D. W. Bardayan, M. Brödeur, S. Coil, and J. J. Kolata, TriSol: A major upgrade of the TwinSol RNB facility, Nucl. Instrum. Methods Phys. Res. A **1047**, 167784 (2023).

[27] K. Palli, A. Pakou, A. M. Moro, P. D. O'Malley, L. Acosta *et al.*, Quasielastic scattering of ^{7}Be + ^{nat}Zr at sub- and near-barrier energies, Phys. Rev. C **107**, 064613 (2023).

[28] K. Palli, A. Pakou, A. Moro, P. D. O'Malley, L. Acosta *et al.*, Breakup of ^{8}B + ^{nat}Zr at the sub-barrier energy of 26.5 MeV Eur. Phys J.-Web Conf. **304**, 03004 (2024).

[29] I. J. Thompson, Coupled reaction channels calculations in nuclear physics, Comput. Phys. Rep. **7**, 167 (1988).

[30] M. Ichimura, N. Austern, and C. M. Vincent, Equivalence of post and prior sum rules for inclusive breakup reactions, Phys. Rev. C **32**, 431 (1985).

[31] H. Esbensen and G. E. Bertsch, Effects of E2 transitions in the Coulomb dissociation of ^{8}B, Nucl. Phys. A **600**, 37 (1996).

[32] A. J. Koning and J. P. Delaroche, Local and global nucleon optical models from 1 keV to 200 MeV, Nucl. Phys. A **713**, 231 (2003).

[33] J. A. Tostevin, F. M. Nunes, and I. J. Thompson, Calculations of three-body observables in ^{8}B breakup, Phys. Rev. C **63**, 024617 (2001).

[34] R. Spartà, A. Di Pietro, P. Figuera, O. Tengblad, A. M. Moro *et al.*, Probing proton halo effects in the ^{8}B + ^{64}Zn collision around the Coulomb barrier, Phys. Lett. B **820**, 136477 (2021).

[35] Jin Lei, `SMOOTHIE` code (unpublished).

[36] P. R. S. Gomes, J. Lubian, I. Padron, and R. M. Anjos, Uncertainties in the comparison of fusion and reaction cross sections of different systems involving weakly bound nuclei, Phys. Rev. C **71**, 017601 (2005).

[37] L. F. Canto, P. R. S. Gomes, J. Lubian, L. C. Chamon, and E. Crema, Disentangling static and dynamic effects of low breakup threshold in fusion reactions, J. Phys. G: Nucl. Part. Phys. **36**, 015109 (2009).

[38] O. Sgouros, V. Soukeras, K. Palli, and A. Pakou, Global approach for the reactions ^{7}Be + ^{28}Si and ^{7}Be + ^{208}Pb at near- and sub-barrier energies, Phys. Rev. C **106**, 044612 (2022).

[39] A. Gómez Camacho, J. Rangel, and J. Lubian, Influence of the capture of breakup fragments on the fusion of 8B with several targets, Phys. Rev. C, **111**, 014604 (2025).

[40] O. Sgouros, A. Pakou, D. Pierroutsakou, M. Mazzocco, L. Acosta *et al.*, α and ^{3}He production in the ^{7}Be + ^{28}Si reaction at near-barrier energies: Direct versus compound-nucleus mechanisms, Phys. Rev. C **94**, 044623 (2016).

[41] O. C. B. Santos, R. L. Filho, K. C. C. Pires, U. Umbelino, E. O. N. Zevallos, A. L. deLara, A.S . Serra, V. Scarduelli, J. Alcantara-Nunez, A. Lepine-Szily, A. M. Moro, S. Appannababu, M. Assuncao, and J. Lei, Elastic scattering and ^{7}Li production in the ^{8}Li + ^{120}Sn reaction, Phys. Rev. C **110**, 034610 (2024).

[42] E. F. Aguilera, J. J. Kolata, F. M. Nunes, F. D. Becchetti, P. A. DeYoung *et al.*, Transfer and/or breakup modes in the ^{6}He + ^{209}Bi reaction near the Coulomb barrier, Phys. Rev. Lett. **84**, 5058 (2000).